INDERSCIENCE PUBLISHERS
Linking academia, business and industry through research

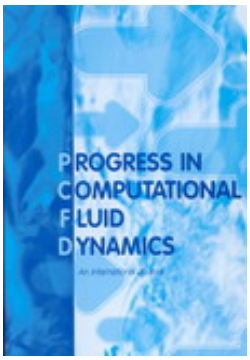

Progress in Computational Fluid Dynamics, An International Journal

ISSN online: 1741-5233 - ISSN print: 1468-4349
https://www.inderscience.com/pcfd

Computational investigation and parametric design of high speed evacuated tube transportation

Arnav De, Sanket Sanjay Nangare, Sreeja Sadasivan, Senthil Kumar Arumugam, Bibin John, Zhang Yaoping

DOI: 10.1504/PCFD.2023.10053759

Article History:

Received:	14 June 2021
Last revised:	04 November 2021
Accepted:	07 November 2021
Published online:	02 February 2023

Computational investigation and parametric design of high speed evacuated tube transportation

Arnav De, Sanket Sanjay Nangare and Sreeja Sadasivan*

School of Mechanical Engineering,
Vellore Institute of Technology,
Tamil Nadu, India
Email: de.arnav@gmail.com
Email: sanket.nangare1998@gmail.com
Email: sreejas66@gmail.com
*Corresponding author

Senthil Kumar Arumugam

School of Mechanical Engineering,
VIT Bhopal University,
Bhopal, 466114, India
Email: asenthilkumar@vit.ac.in

Bibin John

School of Mechanical Engineering,
Vellore Institute of Technology,
Tamil Nadu, India
Email: bibinjohnm@gmail.com

Zhang Yaoping

Institute of Evacuated Tube Transport,
Southwest Jiaotong University,
Chengdu 610031, China
Email: 2285902459@qq.com

Abstract: Evacuated tube transportation is a path-breaking technology that can potentially supplant the current transportation technologies by offering high-speed transportation with maximum efficiency. Different scenarios were considered in which the train was simulated to be travelling at subsonic, transonic, and supersonic speeds at a fixed blockage ratio. It is found that no shockwaves are formed in the subsonic range, but they start forming at the rear end of the train from Mach number 0.8 onwards. From Mach 2, shockwaves start forming at the front end, along the length of the train as well as the rear end of the train. Further, multi-objective optimisation was conducted to evaluate the best combination of various influential factors. One of the salient conclusions of the present study is that the train with the oblique front end, elliptical rear end along with 1,000 Pa tube pressure gives the best combination, resulting in minimum drag.

Keywords: design of experiments; evacuated tube transportation; Mach number; aerodynamic drag; shockwave.

Reference to this paper should be made as follows: De, A., Nangare, S.S., Sadasivan, S., Arumugam, S.K., John, B. and Yaoping, Z. (2023) 'Computational investigation and parametric design of high speed evacuated tube transportation', *Progress in Computational Fluid Dynamics*, Vol. 23, No. 1, pp.13–23.

Biographical notes: Arnav De is an undergraduate student of Vellore Institute of Technology, India.

Sanket Sanjay Nangare is an undergraduate student of Vellore Institute of Technology, India.

Sreeja Sadasivan is an Assistant Professor in the Department of Mechanical Engineering, Vellore Institute of Technology, India. Her research areas include vacuum tube transportation, CFD, multi-phase flow analysis and, turbine exhaust system design.

Senthil Kumar Arumugam is a Professor of Mechanical Engineering at Vellore Institute of Technology, India. His research topics include CFD, cryogenics and, thermal science.

Bibin John is an Associate Professor of Mechanical Engineering, Vellore Institute of Technology, India. His research interests include enhanced heat transfer and CFD solver development for high-speed compressible fluid flow and heat transfer.

Zhang Yaoping is the Founder and Director of the Vacuum Tube Transport Institute of Xijing University, in Xi'an of China. He is working in the area of vacuum tube transportation.

1 Introduction

ETT is the latest evolving transportation technology which has the potential to completely disrupt the current high-speed transportation technologies. In the present scenario, air transportation is the fastest available mode of transportation. However, if we consider the ground mode of transportation, high-speed trains hold the record of travelling at the highest possible speeds. The major speed limiting factor for any high-speed train is the aerodynamic drag induced by the atmosphere in which the train is travelling. Air transportation gets rid of this speed limiting factor to some extent in travelling at a higher elevation from the Earth's surface, where the density of air is very less, which results in a huge reduction in the aerodynamic drag. ETT tries to implement the same idea by proposing a mode of transportation in which a train travels inside a partially evacuated vacuum tube.

High-speed trains have evolved over a long period of time. Initially, in the first generation, the maximum speed achieved was around 250 km/h. In the second generation, the speeds gradually reached up to 300 km/h. Finally, in the third generation of evolution, high-speed trains achieved a speed of around 350 km/h (Zhou and Shen, 2011). It was found that at speeds beyond 300 km/h, the aerodynamic drag accounted for more than 80% of the total drag faced by the train. The only way to reduce this drag is by extensively optimising the design of high-speed trains to make them highly aerodynamic (Yang et al., 2012). Many researchers have undertaken studies on the aerodynamic characteristics of high-speed trains. The main parameter which is studied thoroughly is aerodynamic drag (Zheng et al., 2011). Various parameters which affect the aerodynamic drag are nose shape, nose length, tail shape, tail length, and train length (Niu et al., 2018).

The four key parameters which affect the aerodynamic drag generation in ETT are blockage ratio, internal tube pressure, shape, and speed of the train (Bibin and Mukherjea, 2013; Xiao et al., 2008). It has been found that the total drag is minimum at an internal tube pressure of 1,000 Pa and a blockage ratio of 0.25 (Chen et al., 2012; Zhang, 2012). Similarly, it has been established that aerodynamic drag increases gradually from 1 to 10,000 Pa, but it increases rapidly, or rather exponentially when the internal tube pressure is increased beyond 10,000 Pa. However, very few researches have been conducted to understand how the aerodynamic drag varies when the tube pressure is in the range of 1 to 10,000 Pa. Research has been carried out to understand the change in flow behaviour inside the tube with the increasing speed of the train. For every possible combination of blockage ratio, internal tube pressure, and train geometry, there is some critical speed after which shockwaves start forming inside the tube (Gillani et al., 2019; Kim et al.., 2011). The formation of shockwaves causes a significant effect on various flow parameters and the flow behaviour inside the tube (Niu et al., 2019; Zhou et al., 2019a, 2019b, 2020, 2021; Jang et al., 2021). However, there exists a research gap as very little research has been conducted to understand the mutual interaction of these key parameters.

In the present numerical analysis, CFD Analysis of ETT is conducted using ANSYS Fluent Software. In the first phase of the study, a cylindrical body with an elliptical head and tail is considered to be travelling inside an evacuated tube having an internal tube pressure of 1,000 Pa. The blockage ratio considered for the study is 0.25. The speed of the train is varied according to Mach numbers in the subsonic, transonic, and supersonic range. Various flow parameters are then studied to understand the flow behaviour around the train. Based on the results obtained in the initial study, two further studies are conducted. In the second phase of the present research, nine train geometries are simulated to be travelling at Mach 2.0 but with different combinations of internal tube pressures of 1,000 Pa, 3,000 Pa, and 5,000 Pa. Later, Taguchi's method is used to interpret the results obtained from the second study. This study is carried out to understand the mutual interaction of the shape of the train and internal tube pressure at supersonic speeds and to arrive at optimum train geometry of the train for supersonic evacuated tube transportation.

2 Computational modelling

In the present research, the minimum pressure used in the design of the ETT system is 1,000 Pa. To check the applicability of continuum mechanics, the Knudsen number is calculated by using the equation (1).

$$Kn = \frac{\lambda}{L} \tag{1}$$

where 'λ' and 'L' denote the mean free path of the molecules and the characteristic length of the geometry. For the lowest tunnel operating pressure of 1,000 Pa and temperature of 288.15 K, the Knudsen number obtained with the tube diameter 7.4 m as the characteristic length is

8.5×10^{-5}. Therefore, the working fluid, air in the tube, can be considered as a continuum, and the standard flow governing equations of continuous flowfield, the continuity, momentum, and energy equations can be solved to predict the aerodynamic loads on the train model.

Finite volume-based solver ANSYS Fluent is used to conduct the simulations in the study. The mass, momentum, and energy equations along with the standard k-ε turbulence model are solved in the computational domain. A wall function is used in this model to bridge the variations of flow variables between the viscous affected near-wall region with the fully turbulent region. The value of y^+ is maintained between 30 to 180 to predict the accurate flow variations. The flow behaviour is considered to be viscous, steady, and compressible. The numerical experiments were conducted using density based solver. The least squares cell-based method is used for gradient calculations. Second-order upwind scheme is employed for the discretisation of flow and turbulence parameters. The courant number used for the simulations is 0.5. The residuals of mass, momentum, energy and turbulence terms were set to 1×10^{-6} as the converging criteria.

2.1 Geometry and meshing details

A three-dimensional evacuated tube system is considered in the initial study of the present numerical analysis is shown in Figure 1. The length and diameter of the tube are taken as 329 m and 7.4 m respectively. The length and diameter of the train are taken as 59 m and 3.7 m respectively, which results in a blockage ratio of 0.25. For train shapes of symmetry, the third dimension can be obtained by revolving the solution domain by 360°. Details of the geometry are mentioned in the half sectional view of the ETT system, shown in Figure 2. During the first phase of the research, the shape of the front and the rear ends of the train is taken as elliptical with an eccentricity of 2:1. A structured mesh was generated in the computational domain using mesh generation software ICEM CFD.

Figure 1 Three dimensional geometry of ETT system

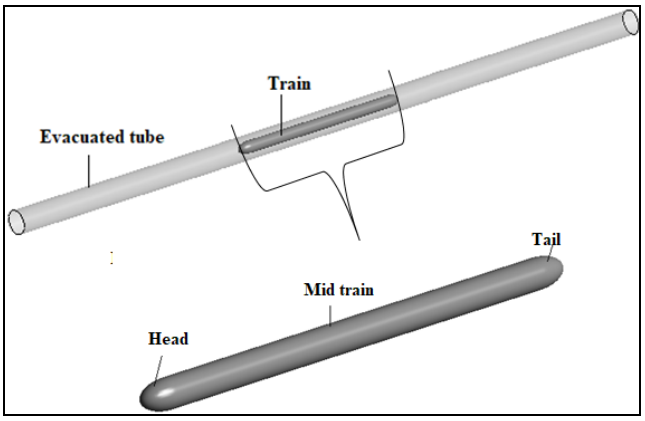

2.2 Boundary conditions

In the present numerical analysis, there are four major boundaries: inlet boundary, train boundary, tube boundary and outlet boundary (Table 1). Each of these boundaries are defined according to the following boundary types.

Figure 2 Geometry details (half sectional view)

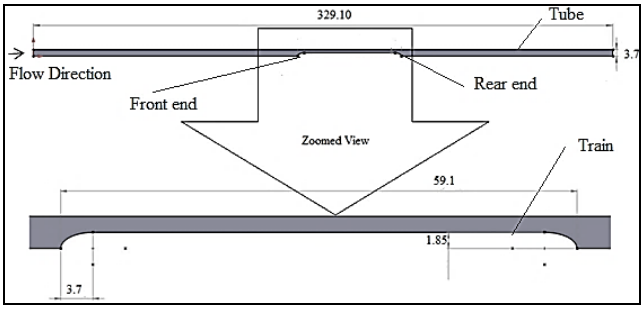

Table 1 Boundary conditions specified at the various parts of the domain

Boundary	*Boundary type*	*Boundary type details*
Inlet	Pressure far field	• Mach number is varied according to the speed of the train
Train	Wall	• Wall motion – stationary wall • No-slip condition
Tube	Wall	• Wall motion – moving wall • Motion – relative to adjacent cell zone • Speed – varied according to Mach numbers • No-slip condition
Outlet	Pressure outlet	• Gauge pressure is kept equal to the internal tube pressure

2.3 Grid independence study

A grid independence study was carried out for both two-dimensional and three-dimensional computational domains to avoid the grid-resulted error in the solution. However, for the reasons of brevity, only 3D grid independence is presented here. The 3D computational domain has been discretised with three different levels of grids, namely, coarse, medium, and fine to carry out the grid-independence study. The number of elements contained in the different levels of the grid is presented in Table 2. To verify grid independence, the pressure distribution over the train boundary was plotted for all three meshes. It can be seen in Figure 3 that there is a slight variation in the pressure values obtained from the coarse mesh compared to that of the medium mesh and the fine mesh. On the other hand, the pressure distributions obtained on the medium and fine grids are nearly identical. Thus, a medium-level grid refinement is noted to be sufficient enough to accurately predict the train aerodynamics of present interest, and the result obtained on that domain can be taken as a grid-independence solution. Therefore, for further calculations, grid refinement corresponding to medium level was used. The mesh used for the model with medium size is depicted in Figure 4.

Table 2 Number of elements contained in different grid levels

Mesh type	*Number of elements*
Coarse	512,531
Medium	738,368
Fine	973,618

Figure 3 Static pressure distribution along the train

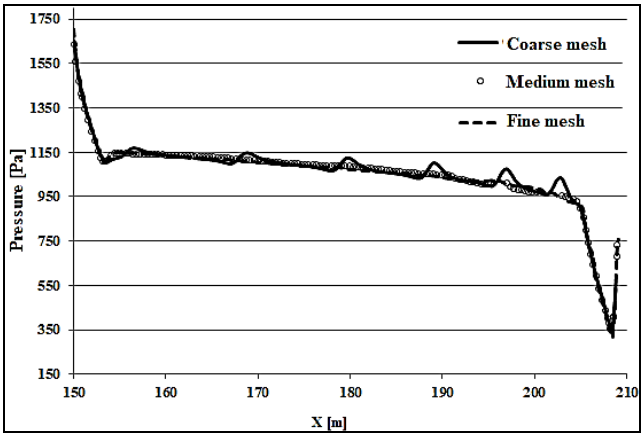

Figure 4 Computational mesh used in the study, (a) 3D (b) half sectional view

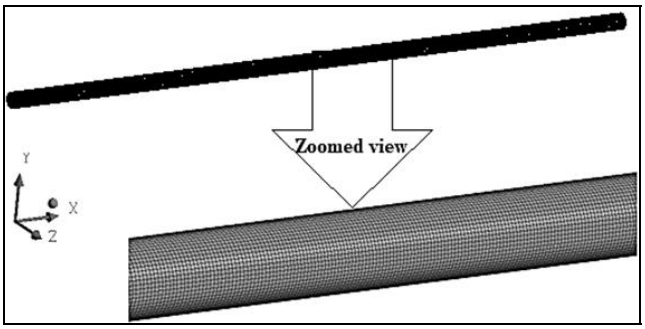

(a)

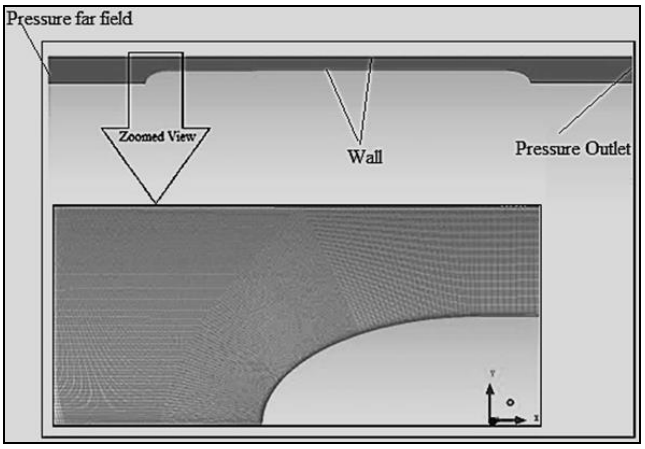

(b)

3 Comparison of 2D-axisymmetric and 3D

This study aims to understand the effect of dimensionality on ETT aerodynamics. The ETT's train shape can be axisymmetric, resulting in a symmetric flow field surrounding the train while travelling at high speeds. In such a case, a full three-dimensional simulation and a reduced 2D-axisymmetric simulation can yield the same results. The flow structure and aerodynamic loads predicted by both the simulation framework would be identical. Therefore, one can opt for the reduced-order model, 2D axisymmetric simulation, for analysing the dynamics of the ETT system having an axis of symmetry. This ensures accurate predictions at a reduced computational cost. However, it is essential to verify the correctness of this argument by comparing the results of two different simulation frameworks mentioned before. Therefore, simulations are carried for case 1 (elliptic head and tail) by employing both 3D and 2D-axisymmetric simulation frameworks. The computational domains used for the 2D and 3D simulations had 50,921 quadrilateral elements and 738,368 hexahedral elements, respectively. The pressure distribution and velocity contours obtained with two different simulation setups are compared in Figures 5 and 6, respectively. It can be noted that the predictions obtained from 3D simulation and 2D-axisymmetric simulation are exactly similar.

Figure 5 Static pressure distribution along the train

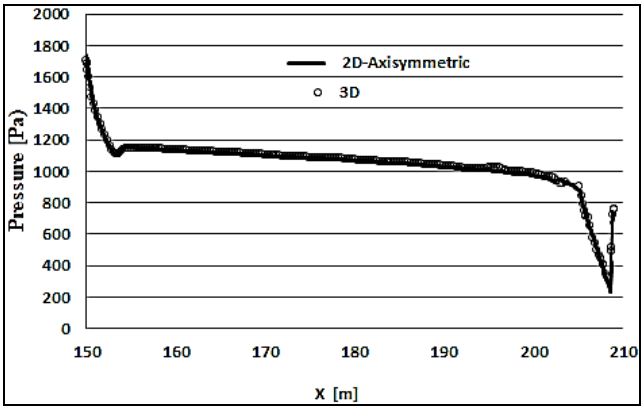

Figure 6 Comparison of velocity contours (a) 2D-axisymmetric (b) 3D (see online version for colours)

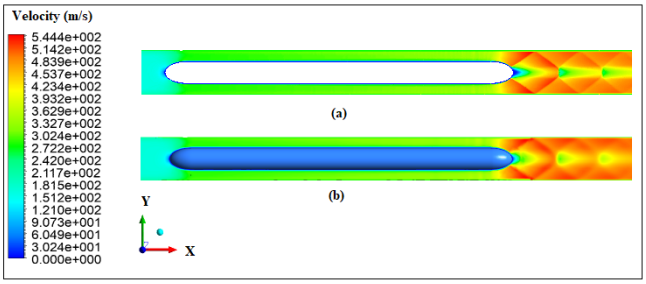

The velocity contours presented in Figure 7(a) clearly show the axisymmetric nature of the flowfield. The contours obtained on the X-Y plane and Z-X plane are the same [Figure 7(b)]. Moreover, the contours shown on the X-Y plane of the 3D domain and planar domain of the 2D-axisymmetric case are very identical. The lower order CFD model could predict the complex shock structure exactly as that obtained from the 3D simulation. Therefore,

2D axisymmetric simulations were performed for the ETT system with axisymmetric train models. On the other hand, for the train models with no specific axis of symmetry, full 3D simulations were performed to calculate the aerodynamic forces.

Figure 7 Velocity contours, (a) perspective view of XY and ZX planes (b) XY plane, ZX plane (see online version for colours)

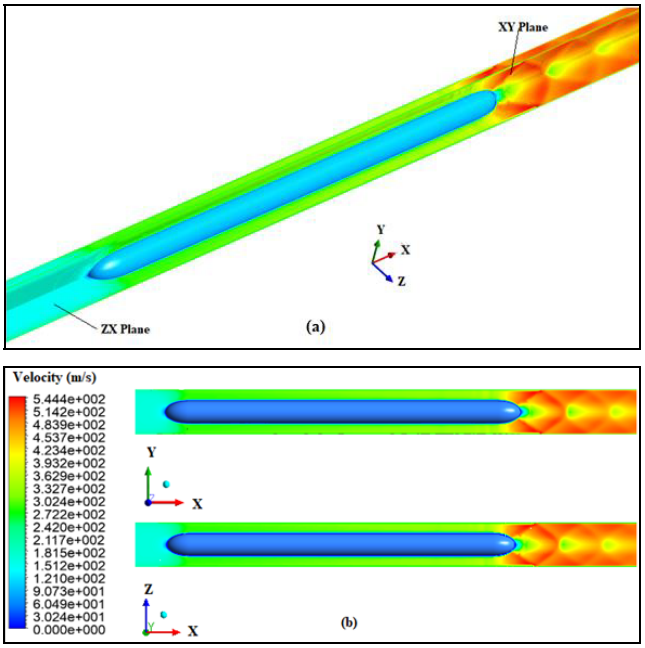

4 Results and discussion

4.1 Effect of Mach number variation on the flow structure in the ETT system

During the first phase of the present study, elliptical head and tail geometry with a major axis to minor axis ratio of 2:1 is used. This train geometry is simulated to travel inside an evacuated tube having an internal tube pressure of 1,000 Pa. A blockage ratio of 0.25 is selected for this study. The train was simulated to travel at subsonic, transonic, and supersonic speeds. The speed of an elliptical head and tail geometry varied from Mach 0.6 to Mach 2.4 with 1,000 Pa internal tube pressure.

The pressure and velocity contours obtained at Mach 0.6 are depicted in Figures 8(a) and 9(a) respectively. It can be observed that there is no shock wave formation when the train is moving at Mach number 0.6. When the train reaches Mach number 0.8, the flow acceleration between the tube and train attains supersonic speed towards the rear end of the train. Subsequent deflection of this supersonic flow at the rear end of the train causes the formation of shock waves at the wake of the train. It is also observed from Figures 8(b) and 8(c) that the shock waves forming at the rear end of the train intensify with the increasing speed of the train. From the pressure contours (Figure 8), it can be noticed that the pressure increases across the shock waves due to the flow deceleration. These shockwaves continue to travel far off the rear end of the train, resulting in intense point stresses at some particular points inside the tube. When the train starts to travel at a speed higher than sonic speed, the dynamics of ETT get changed completely. In this case, the supersonic speed of the train causes the formation of a normal shock within the tube, well ahead of the train nose. The flow further accelerates and attains supersonic speed within the passage between the tube and train. This trend is consistent till Mach 1.8 but after that from Mach 2.0 onwards, the front normal shock starts to recast as bow shockwave as shown in Figure 8(h). From Mach 2.2 onwards, the shockwaves intensify with increasing speed. These shockwaves travel in the space between the train and the tube. Hence, it can be observed that beyond Mach 2, shockwaves will cause intense point stresses both on the train and the tube simultaneously. The corresponding velocity contours obtained for various Mach numbers are depicted in Figure 9.

Figure 8 Pressure contours obtained from different Mach numbers, (a) M = 0.6 (b) M = 0.8 (c) M = 1.0 (d) M = 1.2 (e) M = 1.4 (f) M = 1.6 (g) M = 1.8 (h) M = 2.0 (i) M = 2.2 (j) M = 2.4 (see online version for colours)

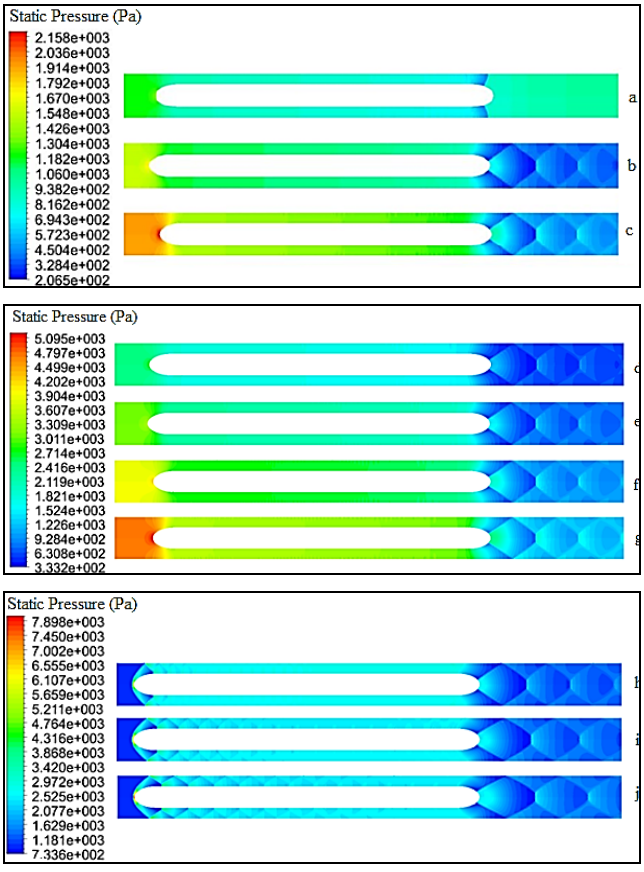

Figure 10 shows that there is very high pressure at the front end of the train which increases as the Mach number increases. When Mach number ranges from 0.6 to 1.8 the pressure rapidly decreases at the front elliptical head of the train after which it decreases almost linearly along the straight length of the train and then again decreases rapidly along the elliptical rear end of the train, before sudden

increase at the rear tip. For above Mach numbers 2.0, it is noticed that the pressure values fluctuate violently at the front end of the train and it is representing the generation of the shockwaves at the front end. The oscillation represents the interaction of shockwaves resulting in the variation of pressure. Similar inference can be obtained from Figure 11. The oscillation in the pressure value along the length of the tube behind the train represents the interaction of shock waves with the tube wall.

Figure 9 Velocity contours obtained from different Mach numbers, (a) M = 0.6 (b) M = 0.8 (c) M = 1.0 (d) M = 1.2 (e) M = 1.4 (f) M = 1.6 (g) M = 1.8 (h) M = 2.0 (i) M = 2.2 (j) M = 2.4 (see online version for colours)

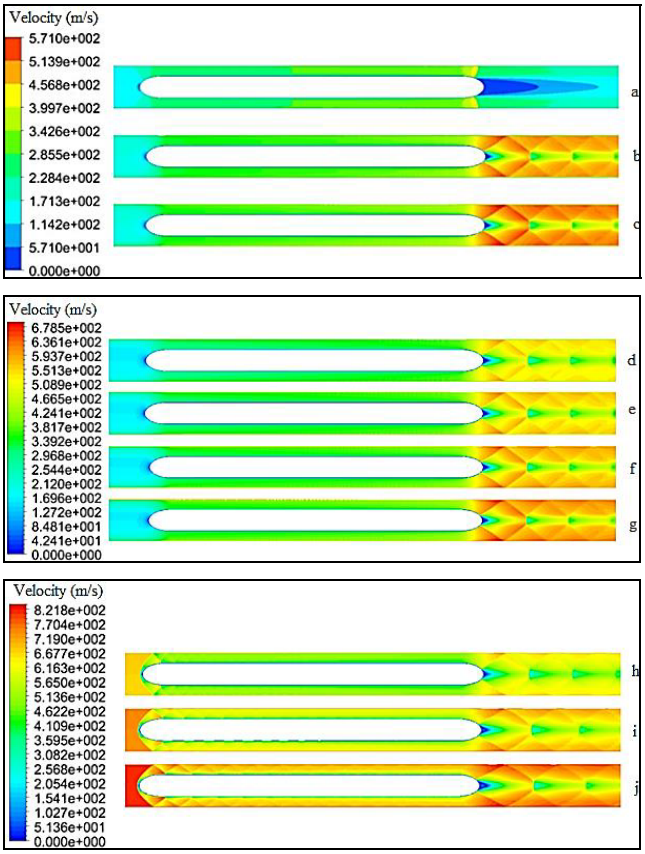

The temperature distribution along the tube is depicted in Figure 12. It is clear from the figure that, when the Mach number is changing from 0.8 to 1.8, the temperature on the surface of the system increases, after which there is a decrease in the temperature along the train due to the formation and interactions of the shockwaves with the train.

From Figure 13, it can be inferred that the skin friction coefficient on the train surface increases with the increase in the Mach number of the system till Mach number 1.8. After that, it can be noticed that the skin friction coefficient starts to decrease when the Mach number is 2 and along the length of the train it is just a little less than the skin friction coefficient value of Mach number 1.8. Beyond Mach number 2, the skin friction coefficient on the tube after the rear end of the train is inversely proportional to the Mach number.

Figure 10 Pressure distribution along the evacuated tube train (see online version for colours)

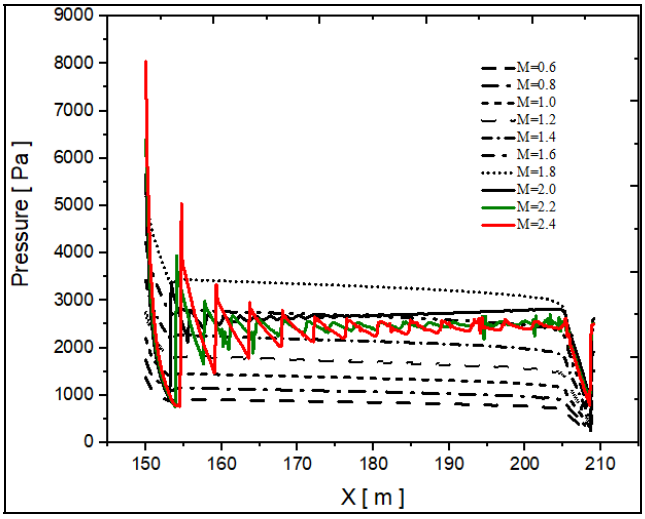

Figure 11 Pressure distribution along the tube (see online version for colours)

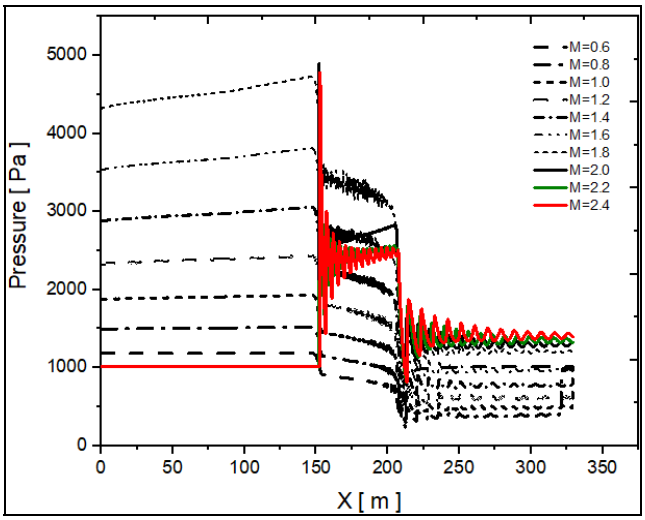

Figure 12 Temperature distribution along the tube (see online version for colours)

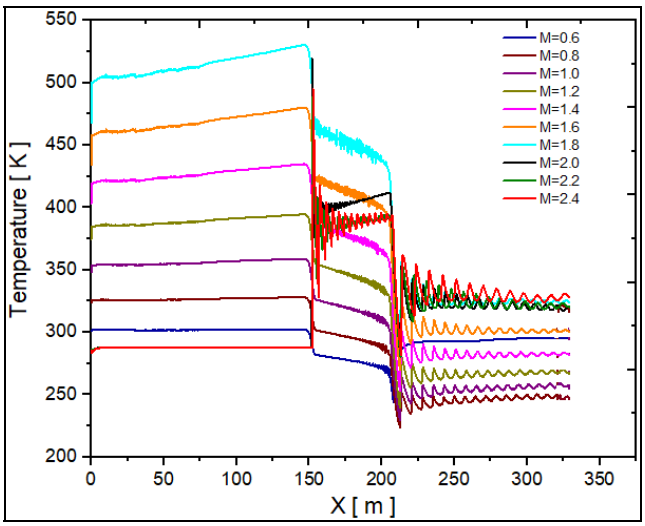

Figure 13 Skin friction coefficient along the tube (see online version for colours)

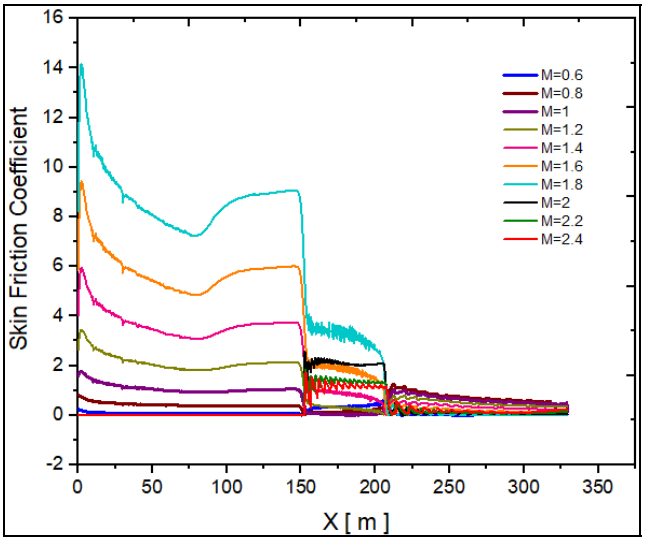

Table 3 Drag values for various Mach numbers

Sl no.	*Mach number*	*Reynolds number (10^6)*	*Pressure drag (N)*	*Total drag (N)*
1	0.6	1.02247	3,919	4,798
2	0.8	1.36329	10,202	11,304
3	1.0	1.70412	12,928	14,266
4	1.2	2.04494	16,254	17,872
5	1.4	2.38577	20,276	22,261
6	1.6	2.72659	25,179	27,640
7	1.8	3.06742	31,134	34,208
8	2.0	3.40824	9,668	12,843
9	2.2	3.74906	12,992	16,778
10	2.4	4.08988	17,073	23,533

Figure 14 Total drag for the various Mach numbers (see online version for colours)

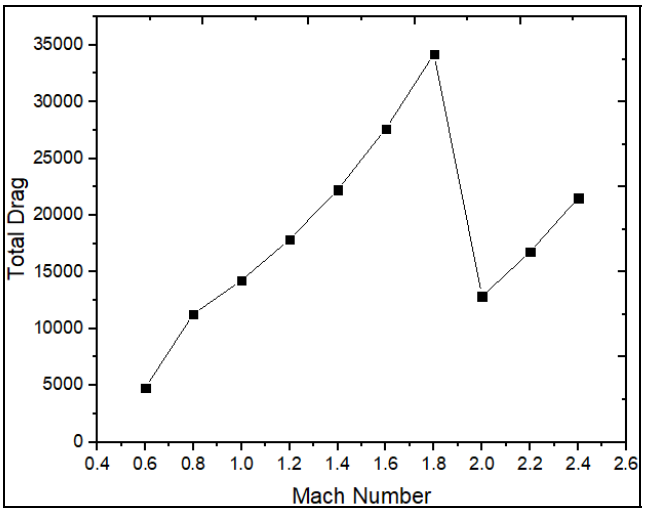

Total pressure drag is an important factor which can predict the performance of evacuated tube transportation. The total pressure drag values obtained from the various Mach number flow simulations are tabulated in Table 3. It is also clear from Figure 14 that the aerodynamic drag increases as the Mach number of the train increase up to 1.8. Subsequently, the rate of change of increment in drag is impeded at the transition from Mach 1.8 to 2.0. This could be due to the formation of a strong bow shock wave ahead of the train and the subsequent shock reflections happening between the train wall and the tube. Further increase in Mach number steadily increases the drag.

5 Optimisation technique

5.1 Taguchi's design of experiments

Taguchi's design of experimentation strategy expects to accomplish an aspiring incentive by decreasing the deviation of parameters affecting aggressive worth. A quadratic mathematical equation is utilised by Taguchi strategy to evaluate the loss of value whenever the fluctuation of parameters varies from its focused targets. It is considered as the signal to noise (SN) ratio. The extraordinary significance of the SN ratio is that it blends both the scattering and the position of a reaction variable as feedback, while remaining strategies examine mean and deviation as split reactions. In Taguchi strategy, the feedback for the most part is classified into three categories, for example, Larger-the-better (LTB), nominal-the-best (NTB), and smaller-the-better (STB). The equation for computation of SN ratio (η_{ij}) for j^{th} response comparing to i^{th} preliminary ($j = 1, 2, \ldots, p$; $i = 1, 2, \ldots, m$) are shifting for different sorts of reactions. The smaller-the-better strategy was adopted in the present optimisation study of the ETT system.

- For LBT responses variable

$$S/N\ ratio = -10\log_{10}\left(\frac{1}{n}\right)\sum_{i=1}^{n}\frac{1}{Y_{ij}^2}$$

- For STB responses variable

$$S/N\ ratio = -10\log_{10}\left(\frac{1}{n}\right)\sum_{i=1}^{n}Y_{ij}^2$$

- For NTB responses variable

$$S/N\ ratio = -10\log_{10}\left(\frac{Y_{ij}^-}{Y_{ij}^2}\right)$$

In the second phase of the research, the design of experiments technique is used to understand the mutual interaction of internal tube pressure along with the shape of the front and the rear end of the train at a constant Mach number. Mach 2.0 is chosen as the speed of the train. Nine different cases were considered with different combinations of the shape of the train and internal tube pressure. All the cases were simulated to compare and analyse the results to find an optimum combination of the shape of the train and internal tube pressure.

Figure 15 Overview of used geometries, (a) geometries used for the design of experiments (b) perspective views of asymmetric 3D geometries (see online version for colours)

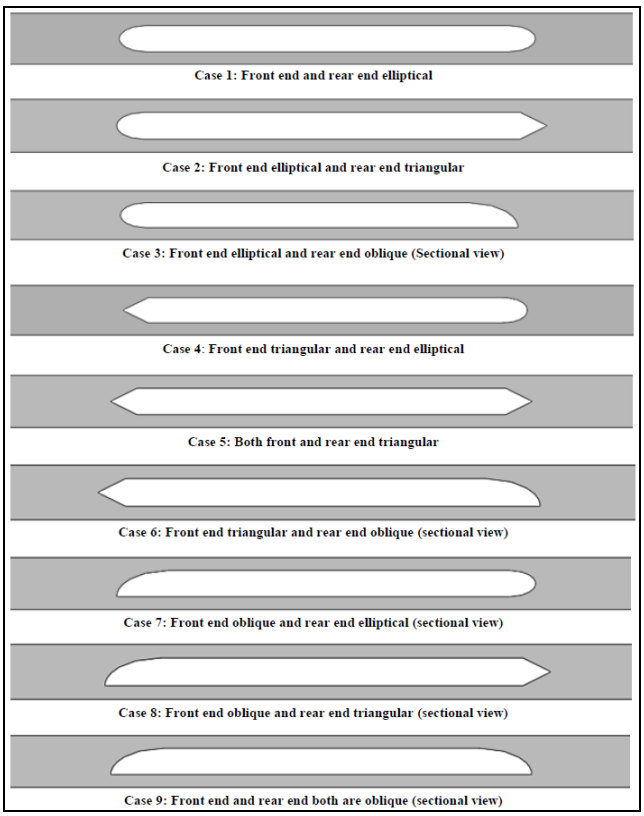

(a)

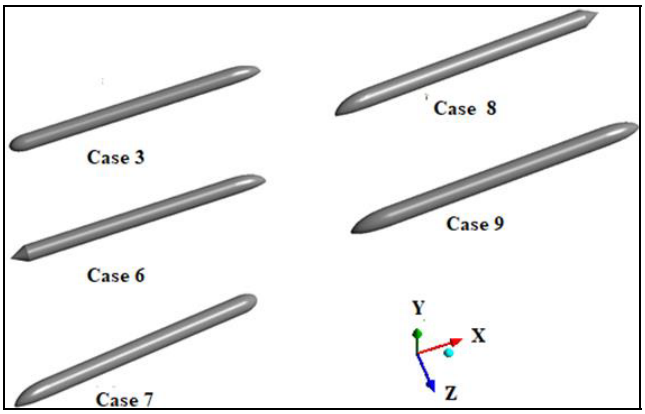

(b)

Initially, a Taguchi DOE table is fabricated as tabulated in Table 4 using Taguchi design which considers various influencing operational parameters like the front end of the train, the rear end of the train, and the operating pressure. The nine different cases and geometries used for the simulations are depicted in Table 5 and Figure 15 respectively. In the present investigations, Cases 1, 2, 4, and 5 have been solved by considering the 2D-axisymmetic nature of the flowfield. Whereas, cases 3 and 6 to 9 were solved in 3D due to their asymmetric nature of the geometry. Regardless of the symmetric/asymmetric nature of the train, the evacuated tube cross-section was maintained as circular in all the simulations. The circular tubes are preferred due to their higher structural integrity and practical installation easiness.

Table 4 Taguchi three-level parameters

Symbol	*Parameters*	*Level*		
		Level 1	*Level 2*	*Level 3*
A	Front end	Elliptical	Triangle	Oblique
B	Back end	Elliptical	Triangle	Oblique
C	Pressure (Pa)	1,000	3,000	5,000

Table 5 Taguchi cases

No.	*Front end*	*Back end*	*Pressure (pa)*
1	Elliptical	Elliptical	1,000
2	Elliptical	Triangle	3,000
3	Elliptical	Oblique	5,000
4	Triangle	Elliptical	3,000
5	Triangle	Triangle	5,000
6	Triangle	Oblique	1,000
7	Oblique	Elliptical	5,000
8	Oblique	Triangle	1,000
9	Oblique	Oblique	3,000

5.2 Results and discussions of design of experiments

To determine the effect of the most influencing parameters on the aerodynamic drag of the train, nine numerical simulations were conducted and responses are presented in Table 6. The average values of drag for each parameter at levels 1, 2, and 3 are calculated and tabulated in Table 7. It is seen that the total drag experienced on the train increases with the increase in the pressure value. When compared to this vast variation in the pressure, the shape of the front and the rear ends of the train impart significantly less effect. The influence of the shape of the rear end on the drag is slightly higher than that of the shape of the front end of the train. Moreover, in all the cases normal shock waves coexist with the oblique shock waves that are generated due to the reflection and interaction of shock waves between the train wall and the tube wall. Figure 16 represents the main effects plot of total drag on the train by considering the influential factors, the front end of the train, the rear end of the train, and operating pressure. The above-stated discussion is more evident from the main effects plot of the total drag (Figure 16).

From the normal probability plot in Figure 17, it can be concluded that the regression equation obtained is correct since the points representing the results from the simulation lie very close to the line of regression. Also, from the versus order plot, it can be stated that there is no pattern is being formed in the graph; the parameters considered in the study are mutually independent of each other. From Table 8, it can be noticed that the internal tube pressure has the lowest p-value. Therefore, it can be concluded that it is the most

influencing parameter, followed by the rear end shape of the train and then the front end shape of the train.

Table 6 Taguchi experimental analysis

No.	*Front end*	*Back end*	*Pressure (Pa)*	*Total drag (N)*
1	Elliptical	Elliptical	1,000	12,843
2	Elliptical	Triangle	3,000	19,082
3	Elliptical	Oblique	5,000	66,226
4	Triangle	Elliptical	3,000	20,859
5	Triangle	Triangle	5,000	70,695
6	Triangle	Oblique	1,000	14,177
7	Oblique	Elliptical	5,000	55,534
8	Oblique	Triangle	1,000	12,534
9	Oblique	Oblique	3,000	23,656

Figure 16 Main effects plot for drag (see online version for colours)

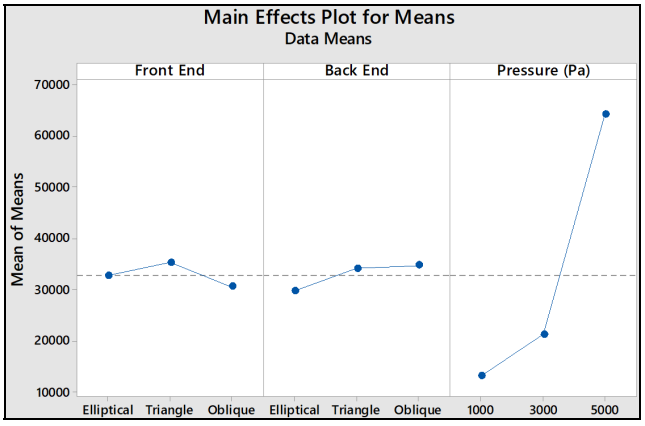

Table 7 Response table for means

Level	*Front end*	*Back end*	*Pressure (Pa)*
1	32,717	29,745	13,185
2	35,244	34,104	21,199
3	30,575	34,686	64,152
Delta	4,669	4,941	50,967
Rank	3	2	1

Table 8 Analysis of variance

Source	*DF*	*Contribution*	*Adj. SS*
Front end	2	0.71%	32,773,198
Back end	2	0.94%	43,748,051
Pressure (Pa)	2	97.12%	4,506,796,202
Error	2	1.23%	57,019,967
Total	8	100.00%	
Source	*Adj. MS*	*F-value*	*P-value*
Front end	16,386,599	0.57	0.635
Back end	21,874,025	0.77	0.566
Pressure (Pa)	2,253,398,101	79.04	0.012
Error	28,509,983		
Total			

Out of the three different parameters small the better type has been chosen in the design of experiments. The least value of aerodynamic drag obtained from each factor was taken into account from the analysis. The best optimal combination obtained from the analysis is 'front end-oblique, back end-elliptical, pressure-1,000 Pa'. The calculated value of drag for the optimal combination is A-3, B-1, C-1, using the Taguchi design approach.

Figure 17 Residual plot for drag (see online version for colours)

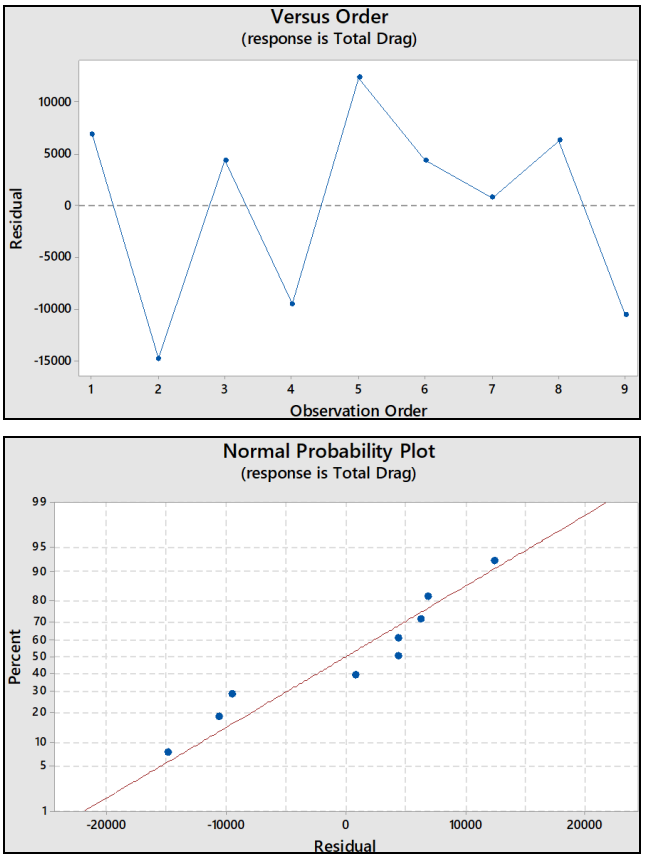

The aerodynamic drag decreases with the decrease in internal tube pressure. However, the further decrease in internal tube pressure will be very expensive or it is very difficult to achieve for the entire length of the tube. Hence, it is recommended to keep the pressure in the tube about a hundred times lesser than the P_{atm}. The geometry of the optimal combination is depicted in Figure 18. These optimised parameters resulted in a minimum drag value of 11,548 N. The shock wave interactions obtained for the above case are shown in Figure 19.

Three-dimensional studies performed for the asymmetric train models revealed the dissimilar flow structure at the different reference planes. It is evident from the velocity and pressure contours at XY and ZX planes of the ETT system (Figures 20 and 21). In the case of the symmetric ETT system, the flow structure is not different in both the reference planes. The main disparity exists at the leading edge region of the asymmetric train model. The bow shock created due to high-speed travel of the train is highly asymmetric in the optimised case. Since the shock has a much-reduced strength in the lateral planes, the drag

obtained for this model was noted to be less. Therefore, the flow asymmetry induced by the train shapes having no axis of symmetric proved to be yielding aerodynamic benefits. However, weight distribution, vehicle stability, and control may be a bit more complex when asymmetric train models are used in the real ETT systems.

Figure 18 Optimised geometry, (a) geometry details (b) perspective view (see online version for colours)

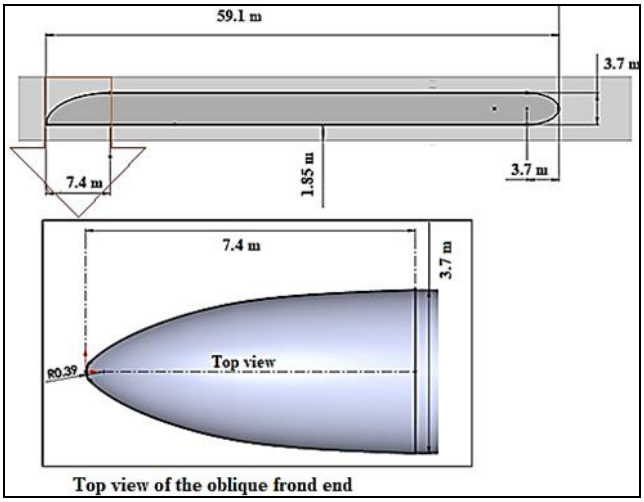

(a)

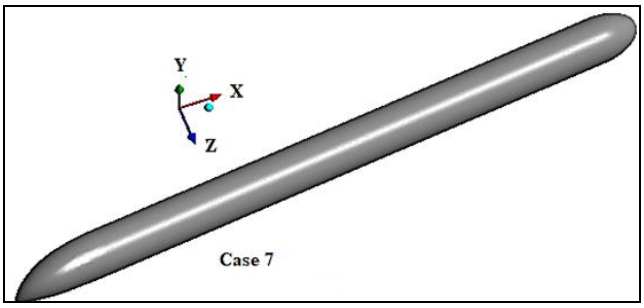

(b)

Figure 19 Velocity contours obtained in the XY and ZX planes of the optimised geometry (see online version for colours)

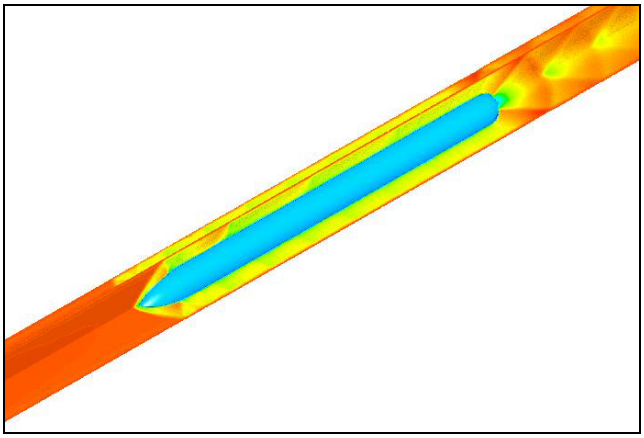

Figure 20 Velocity contours in XY and ZX planes (see online version for colours)

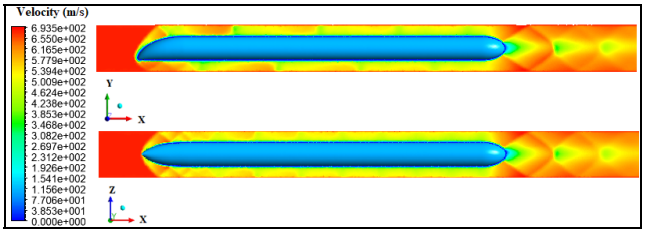

Figure 21 Pressure contours in XY and ZX planes (see online version for colours)

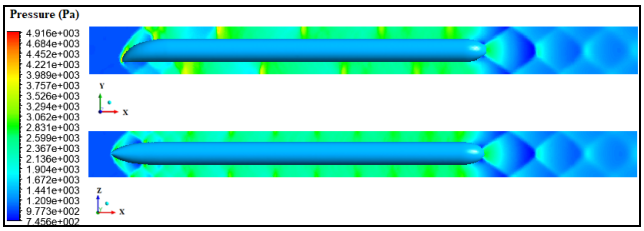

6 Conclusions

The overall objective of this research was to investigate and identify the optimal design and operating conditions for high-speed evacuated tube transportation. This has been done by conducting CFD simulations and applying Taguchi's algorithm on those results to get the desired conclusion.

From the Mach number variation study, it was inferred that although there is a uniform increase in the pressure loss with the increase in Mach number, there is a dip in the gradient of increase when transitioning the flow from Mach 1.8 to Mach 2.0. This can be attributed to the conversion of front shock from normal to curved/bow shape and subsequent formation of shock trains in the spacing between the train and tube when the train speed is within specified Mach number range. Similar to pressure, the skin friction value was also continuously increasing with the increase in Mach number. One riveting observation is that the total drag increased steadily as the Mach number was increased from 0.6 to 1.8, but then it suddenly decreased at Mach 2.0 to a value almost equal to the total drag value at Mach 1.0, before starting to again increase uniformly.

Due to the shock wave interaction, a favourable variation was noticed at Mach 2.0. Taguchi's DOE algorithm was then applied to study various parameters at Mach 2.0 to find an optimised train geometry and internal tube pressure. From this study, it was concluded that the best-optimised train geometry is front end – oblique shape with an aspect ratio of 2:1 and rear end – elliptical shape with an aspect ratio of 2:1. It was also concluded that the best operating internal tube pressure is 1,000 Pa with optimal vacuum creation cost. The aerodynamic drag calculated for the optimised case was 11,548 N, which can be considered as the best result from the considered set of parameters.

References

Bibin, S. and Mukherjea, S.K. (2013) 'Numerical investigation of aerodynamic drag on vacuum tube high speed train', in *ASME 2013 International Mechanical Engineering Congress and Exposition*, American Society of Mechanical Engineers Digital Collection, November.

Chen, X., Zhao, L., Ma, J. and Liu, Y. (2012) 'Aerodynamic simulation of evacuated tube maglev trains with different streamlined designs', *Journal of Modern Transportation*, Vol. 20, No. 2, pp.115–120.

Gillani, S.A., Panikulam, V.P., Sadasivan, S. and Yaoping, Z. (2019) 'CFD analysis of aerodynamic drag effects on vacuum tube trains', *Journal of Applied Fluid Mechanics*, Vol. 12, No. 1, pp.303–309.

Jang, K.S., Le, T.T.G., Kim, J., Lee, K.S. and Ryu, J. (2021) 'Effects of compressible flow phenomena on aerodynamic characteristics in Hyperloop system', *Aerospace Science and Technology*, Vol. 117, p.106970.

Kim, T.K., Kim, K.H. and Kwon, H.B. (2011) 'Aerodynamic characteristics of a tube train', *Journal of Wind Engineering and Industrial Aerodynamics*, Vol. 99, No. 12, pp.1187–1196.

Niu, J., Sui, Y., Yu, Q., Cao, X. and Yuan, Y. (2019) 'Numerical study on the impact of Mach number on the coupling effect of aerodynamic heating and aerodynamic pressure caused by a tube train', *Journal of Wind Engineering and Industrial Aerodynamics*, Vol. 190, pp.100–111.

Niu, J., Wang, Y., Zhang, L. and Yuan, Y. (2018) 'Numerical analysis of aerodynamic characteristics of high-speed train with different train nose lengths', *International Journal of Heat and Mass Transfer*, Vol. 127, pp.188–199.

Xiao, Z., Dianye, Z. and Yaoping, Z. (2008) 'Numerical simulation of blockage rate and aerodynamic drag of high-speed train in evacuated tube transportation', *Chinese Journal of Vacuum Science and Technology*, Vol. 6.

Yang, G., Guo, D., Yao, S. and Liu, C. (2012) 'Aerodynamic design for China new high-speed trains', *Science China Technological Sciences*, Vol. 55, No. 7, pp.1923–1928.

Zhang, Y. (2012) 'Numerical simulation and analysis of aerodynamic drag on a subsonic train in evacuated tube transportation', *Journal of Modern Transportation*, Vol. 20, No. 1, pp.44–48.

Zheng, X.H., Zhang, J.Y. and Zhang, W.H. (2011) 'Numerical simulation of aerodynamic drag for high-speed train bogie', *Jiaotong Yunshu Gongcheng Xuebao*, Vol. 11, No. 2, pp.45–51.

Zhou, L. and Shen, Z. (2011) 'Progress in high-speed train technology around the world', *Journal of Modern Transportation*, Vol. 19, No. 1, pp.1–6.

Zhou, P., Qin, D., Zhang, J. and Li, T. (2021) 'Aerodynamic characteristics of the evacuated tube maglev train considering the suspension gap', *International Journal of Rail Transportation*, pp.1–21.

Zhou, P., Zhang, J. and Li, T. (2020) 'Effects of blocking ratio and Mach number on aerodynamic characteristics of the evacuated tube train', *International Journal of Rail Transportation*, Vol. 8, No. 1, pp.27–44.

Zhou, P., Zhang, J., Li, T. and Zhang, W. (2019) 'Numerical study on wave phenomena produced by the super high-speed evacuated tube maglev train', *Journal of Wind Engineering and Industrial Aerodynamics*, Vol. 190, pp.61–70.

Zhou, P., Zhang, J. and Li, T. (2020) 'Effects of blocking ratio and Mach number on aerodynamic characteristics of the evacuated tube train', *International Journal of Rail Transportation*, Vol. 8, No. 1, pp.27–44.

Nomenclature

Latin letters	
DoE	Design of experiments
ETT	Evacuated tube transportation
k	Turbulence kinetic energy
Kn	Knudsen number
L	Characteristics length
M	Mach number
y^+	Wall function
Greek letters	
β	Blockage ratio = (cross-sectional area of the train) / (cross-sectional area of the tube)
ε	Turbulent dissipation ratep
λ	Mean free path of fluid molecules